

Heavy flavor machine learning algorithms for fast data processing in sPHENIX

Cameron Dean*, on behalf of the sPHENIX and FastML collaborations

¹Massachusetts Institute of Technology

Abstract. The sPHENIX experiment at RHIC utilizes the first new heavy ion detector since the switch on of the LHC experiments. It's optimized for precision jet and heavy flavor physics measurements, and recorded its first collisions on May 18th 2023. sPHENIX uses a streaming readout tracking system and barrel calorimeters to reconstruct the collision topology with event plane detectors, minimum bias detectors and zero-degree calorimeters to characterize the event. The streaming readout detectors are capable of recording 10% of the minimum bias rate in $p+p$ collisions which will enable precision b -hadron and heavy flavor jet measurements at RHIC. An AI-assisted hardware trigger demonstrator is under development to sample the remaining 90% of minimum-bias $p+p$ collisions with an aim for further deployment at the EIC.

1 Introduction

On May 18th 2023, the sPHENIX collaboration received permission to operate and started recording Au+Au collisions at the first new heavy ion detector since the switch on of the LHC experiments. sPHENIX consists of four tracking detectors, barrel electromagnetic and hadronic calorimeters along with event plane detectors, minimum-bias detectors and zero-degree calorimeters to fully characterize Au+Au collisions. Combined with a state-of-the-art streaming readout (SRO) system from the tracking detectors, sPHENIX will complete the RHIC science mission with high statistics measurements from open charm, b -hadron and heavy flavor jets along side a wide array of other physics studies. The SRO is designed to record 10% of the minimum bias rate in $p+p$ collisions. A demonstrator module which employs machine-learning algorithms on field-programmable gate arrays (FPGAs) is under development to sample the remaining 90% of the collisions which will complement the base program of sPHENIX.

The innermost detector is the monolithic active pixel sensor vertex detector (MVTX) is a three-layer detector which allows precise vertex determination and primary/secondary vertex separation as it is capable of a track resolution of approximately $5\ \mu\text{m}$ and a 2D-DCA resolution of approximately $30\ \mu\text{m}$ for tracks with a p_T greater than 1 GeV and approaching $10\ \mu\text{m}$ with increasing p_T [1]. After the MVTX is the intermediate tracker (INTT), a silicon-strip detector with a timing resolution of 106 ns. This is aligned with the $p+p$ collision period and hence allows for pile-up separation. The next tracking detector radially is the time-projection chamber (TPC) which records clusters between 30 cm and 80 cm and uses an Argon/CF₄ gas mixture to enable precise momentum determination. The TPC is designed

*e-mail: ctdean@mit.edu

38 to achieve a momentum resolution of less than 125 MeV which will allow for the separation
39 of the three Upsilon S-states [2]. The last tracking system is the Time Projection Outer
40 Tracker (TPOT) which gives a final measurement point and is used to correct for space charge
41 distortions in the TPC.

42 The electromagnetic calorimeter consists of wavelength shifting fibers embedded in a
43 tungsten powder/epoxy mixture to give an energy resolution of $\sigma/E \leq 16\%/\sqrt{E} \oplus 5\%$ [3].
44 The hadronic calorimeters (HCal) are of a shashlik design on either side of the solenoidal
45 magnet, where the inner HCal uses scintillators and aluminum plates and the outer HCal uses
46 steel instead of aluminum. The outer HCal also doubles as the magnets flux return and the
47 combined HCal system is designed to have $\sigma/E \leq 100\%/\sqrt{E}$.

48 When the approval to operate sPHENIX was given on May 18th 2023, the collaboration
49 proceeded with commissioning the detector efficiently and methodically in stages beginning
50 with the minimum-bias detectors and the calorimetry system. The RHIC run in 2023 was
51 planned to continue until September 30th, however the run terminated on August 1st due to
52 a cryogenic valve box failure external to sPHENIX. By this stage the calorimeters, end-cap
53 detectors, INTT and TPOT had been commissioned and studies on the MVTX and TPC were
54 ongoing. In spite of this early end, all subsystems had successfully recorded data and shown
55 internal system correlations and several correlations between subsystems. The sPHENIX col-
56 laboration continued commissioning using cosmic rays and demonstrated correlations among
57 the entire tracking system to be used for detector alignment.

58 2 Open heavy flavor at sPHENIX

59 The collision energy at RHIC compared to the LHC results in an improved sensitivity to
60 the hadronization mechanisms of heavy flavor particles and their interactions with the quark-
61 gluon plasma (QGP), with the mean p_T of the mothers having a lower value at RHIC. This
62 is especially true for b -hadrons with b -quarks having a larger mass than c -quarks and so
63 they experience less recoil from the medium for comparable momenta. The combination of
64 lower center-of-mass energy, DCA resolution from the MVTX and SRO means sPHENIX
65 will make precision measurements of b -hadrons in heavy ion collisions.

66 By using non-prompt D^0 decays, sPHENIX can measure R_{AA} and v_2 in comparison to
67 prompt D^0 decays and give insights into parton energy loss mechanisms. If a Brownian
68 motion-like approach is used to understand the transport of quarks through the QGP, then we
69 can also use v_2 measurements to constrain the heavy quark diffusion coefficients. Projections
70 for the statistical uncertainty on both of these measurements can be seen in figure 1.

71 The large prompt D^0 data-set can be used to understand direct flow in both the D^0 and \bar{D}^0
72 systems where it is expected that the transient magnetic field will cause a splitting in the flow
73 values as the magnetic field operator is odd under charge conjugation [5]. This measurement
74 has been attempted before but was statistically limited [6]. Also complicating the measure-
75 ment is the need to separate the D^0 states. In the $K^\mp\pi^\pm$ final state, which has both a large
76 branching fraction ($\sim 4\%$ [7]) and can be fully reconstructed, the D^0 undergoes mixing [8]
77 and can decay to both final states (known as "right-sign" and "wrong-sign" decays). Tech-
78 niques are being developed at sPHENIX to correct for these challenges which, if uncorrected
79 for, can dilute the splitting effect and mask it entirely if it is small enough.

80 The D^0 production can also be combined with Λ_c^+ reconstruction to look at the baryon-
81 to-meson ratio in both $p+p$ and Au+Au. Previous studies of this ratio using light flavor
82 decays has demonstrated an enhancement in heavy ion collisions compared to $p+p$ collisions.
83 While the STAR collaboration observed a similar ratio in Au+Au collisions using open charm
84 decays, there is no measurement from RHIC using a $p+p$ data set [9]. Using SRO will allow

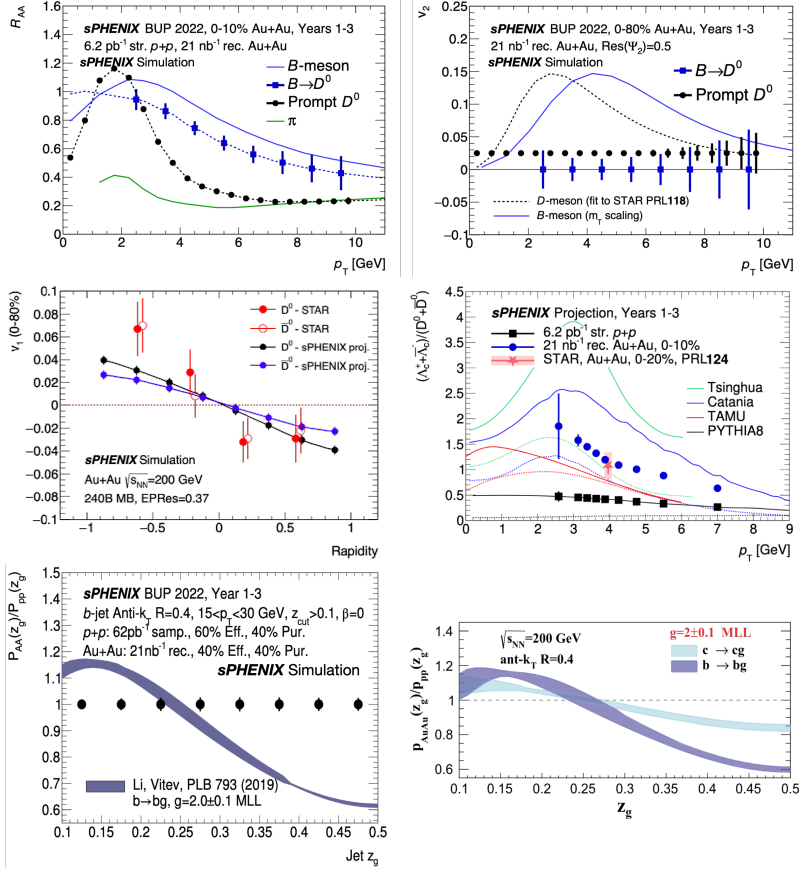


Figure 1. Projected statistical sensitivities to R_{AA} (top left) and v_2 (top right) for prompt (black) and non-prompt (blue) D^0 , sensitivities to v_1 for D^0 and \bar{D}^0 decays (middle left), sensitivity to the baryon/meson ratio in open charm decays (middle right) for $p+p$ (black) and Au+Au (blue), and sensitivity to the sub-jet splitting ratio for b -jets (bottom right) at sPHENIX using 10% SRO. A comparison of the expected enhancement of the sub-jet splitting ratio for c - and b -jets can be seen in the bottom right figure where the enhancement is more prominent for b -jets [4].

85 for a measurement of this ratio in $p+p$ collisions for a direct comparison to the Au+Au
 86 results.

87 sPHENIX also has an extensive heavy flavor jets program such as studying elliptical flow
 88 in the medium p_T regime in the most central events. In the range from approximately 15
 89 to 40 GeV, it is expected that the light and heavy flavor jets exhibit similar flow behavior
 90 and sPHENIX will provide valuable insight as to why these behaviors converge. Another jet
 91 measurement of interest is to compare the sub-jet splitting, z_g , of b -jets in Au+Au and $p+p$
 92 collisions. The splitting can be used as another constraint on the QGP and is expected to be
 93 more prominent in the beauty compared to the charm sector [4].

94 3 AI-assisted event selection

95 The plots shown in figure 1 were produced using the expected statistics recorded with 10%
 96 SRO which is achieved by extending the readout of the tracking system up to 7 μ s after a

97 trigger decision is received during $p+p$ collisions. The back-end electronics of the calorime-
98 try system have a maximum trigger rate of 15 kHz which corresponds to the mean Au+Au
99 collision rate at RHIC, whereas the $p+p$ collision rate is 3 MHz. The data volume is also
100 dominated by the information from the TPC so it was chosen to stream for 7 μ s to avoid over-
101 filling the data buffers. With this in mind, a group are developing a demonstrator model to be
102 deployed at sPHENIX to sample the remaining 90% of $p+p$ collisions using the MVTX and
103 INTT, perform a fast ($\sim 5 \mu$ s) tracklet reconstruction and event selection to identify potential
104 heavy flavor decays. This demonstrator will then send a signal to the TPC to read out its data
105 which will be saved alongside the MVTX and INTT to enhance heavy flavor statistics.

106 The decision unit will consist of a FELIX card ¹ housed inside a standalone server. Data
107 will be passed optically from the MVTX and INTT back-end electronics ² where all the un-
108 packing, clustering, reconstruction and decision making will be performed on the board's
109 FPGA. Tracklet reconstruction and event determination are made using graph neural net-
110 works, and thus the algorithms must be translated to a high level synthesis language. This
111 is achieved by the hls4ml package [10] which performs this translation and synthesizes an
112 IP block which can be placed inside a firmware design. This is advantageous as it allows
113 algorithms to be integrated within other firmware development such as data unpacking and
114 clustering. Another feature of hls4ml is the ability to tune an algorithm between execution
115 speed and precision by altering the number of bits (flip-flops or FF) used in each stage of the
116 algorithm.

117 Conceptually, a graph consists of a set of nodes and related nodes are connected by edges
118 to aggregators. In our model, each node represents a track where a track is represented by 3
119 MVTX and 2 INTT hits, the distance separating hits in adjacent layers, their angle and the
120 summed length of the hit separation. The aggregators represent the vertices and so the edges
121 are used to define which tracks belong to primary or secondary vertices. The neural network
122 passes information from the nodes to the aggregators and back to build weights for each
123 edge until the model builds a full picture of the event. The event selection algorithm is still
124 under development but uses a preliminary model based on secondary vertex determination.
125 The combined tracklet reconstruction and event selection has an average processing time of
126 8.8 μ s with a 285 MHz clock and uses 15% of the FPGA lookup tables, 8% of FFs and 20%
127 of block RAM. Overall this resulted in a 91% tracklet-building efficiency for a 97% area-
128 under-the-curve. The device aims to be deployed at sPHENIX during run-24.

129 References

- 130 [1] The sPHENIX Collaboration, *MVTX Technical Design Report* (2018), [https://](https://indico.bnl.gov/event/4072/)
131 indico.bnl.gov/event/4072/
- 132 [2] The sPHENIX Collaboration, *sPHENIX Technical Design Report* (2019), [https://](https://indico.bnl.gov/event/7081/)
133 indico.bnl.gov/event/7081/
- 134 [3] C.A. Aidala et al., *IEEE Transactions on Nuclear Science* **68**, 173 (2021)
- 135 [4] H.T. Li, I. Vitev, *Physics Letters B* **793**, 259 (2019)
- 136 [5] U. Gürsoy, D. Kharzeev, K. Rajagopal, *Phys. Rev. C* **89**, 054905 (2014)
- 137 [6] J. Adam et al. (STAR Collaboration), *Phys. Rev. Lett.* **123**, 162301 (2019)
- 138 [7] R.L. Workman, Others (Particle Data Group), *PTEP* **2022**, 083C01 (2022)
- 139 [8] R. Aaij et al. (LHCb Collaboration), *Phys. Rev. Lett.* **127**, 111801 (2021)
- 140 [9] J. Adam et al. (STAR Collaboration), *Phys. Rev. Lett.* **124**, 172301 (2020)
- 141 [10] F. Fahim et al., *arXiv* **2103.05579** (2021)

¹BNL-711 or BNL-812

²BNL-712s